

6-10-2022

An Innovative Neutrosophic Combinatorial Approach Towards the Fusion and Edge Detection of MR Brain Medical Images

Premalatha Rathnasabapathy

Dhanalakshmi Palanisam

Follow this and additional works at: https://digitalrepository.unm.edu/nss_journal

Recommended Citation

Rathnasabapathy, Premalatha and Dhanalakshmi Palanisam. "An Innovative Neutrosophic Combinatorial Approach Towards the Fusion and Edge Detection of MR Brain Medical Images." *Neutrosophic Sets and Systems* 50, 1 (2022). https://digitalrepository.unm.edu/nss_journal/vol50/iss1/34

This Article is brought to you for free and open access by UNM Digital Repository. It has been accepted for inclusion in Neutrosophic Sets and Systems by an authorized editor of UNM Digital Repository. For more information, please contact disc@unm.edu.



An Innovative Neutrosophic Combinatorial Approach Towards the Fusion and Edge Detection of MR Brain Medical Images

Premalatha Rathnasabapathy^{1,*} and Dhanalakshmi Palanisami¹

¹Department of Applied Mathematics, Bharathiar University, Coimbatore-641046, TN, India.

E-mail: dhanamath@buc.edu.in

*Correspondence: premalatha.appliedmaths@buc.edu.in

Abstract. This research proposes the idea of implementing an innovative mechanism to detect the edges in distinct MR brain medical images based on the aspect of Neutrosophic sets (NSs). NS-based entropy is one of the emerging tools to procure a neutrosophic image from the crisp image. Followed by the aforementioned procedure, fusion has been done for the neutrosophic image in order to acquire fused neutrosophic images (FNI) then the FNI's are again regenerated to form a fused crisp image. Later, the Bell-Shaped (BS) function and the Sobel operator works on the FNI to obtain a combination of three subsets. After determining the neutrosophic subsets, various entropies such as Norm, Threshold, Sure, and Shannon act on it to provide their threshold values, and the computed subsets along with thresholds are incorporated to produce a new binarized image. Subsequently, morphological operations were implemented to construct the image edges. The resultant images with different entropies are compared by using the performance measurement factors. Based on the measurement factors, the proposed Norm entropy image edge detection innovations have proven to be an efficient tool with reference to other entropies. In addition, the Norm entropy-based proposed method was compared with some of the other existing edge detection methods inclusive of Sobel, Chan, Tian, and Wu. FOM and PSNR factors have been applied to estimate the results of edge detection achieved through five distinct methods. The findings confirmed that the implementation of the proposed object edge detection mechanism is much stronger compared to other existing methods.

Keywords: Neutrosophic set; Image Fusion; Segmentation; Entropy; Edge detection; Homogeneity

1. Introduction

Over the past few decades, two key applications such as image fusion and segmentation have become much clearer and they are significant in the field of image processing and computer

vision, see references [1, 2] for more details. Nowadays, a substantial number of analytically validated image fusion and segmentation, that have been applied to fuse and segment the image objects, and also have been defined to eliminate the noise and its related uncertainty factors. In general, the scheme of fusion is characterized into three parts such as feature, pixel, and decision level. One of the fusion methods is, every pixel of the source images is summed and takes the average then gets the fused image, this algorithm gives the lower performance. So, various types of multi-resolution transform appeared to deal with this problem and they are employed in image fusion. Many image fusion schemes are available, but some schemes are frequently handled, they are spatial fusion, transform fusion, contourlet transform, gradient pyramid, Laplacian pyramid, MSVD, wavelet transform, curvelet transform, etc. The image is fused by the notion of SVD called singular value decomposition that execution is more similar to wavelets. The MSVD based image fusion has been viewed as a faster performance than approximated SVD, see the reference [3] for further details.

Edge detection is a kind of crucial step in the human visual system and image analysis, which is the wild development research area in image processing. The edge detection process substantially alleviates the amount of information because it divides the meaningful data and shields the foremost geometric features. To illustrate the object edges, the object data is performed by either analog / digital computation. The edge is noted as a significant local change in the intensity of the image. In general, the edge is correlated with pixel discontinuity and it occurs between distinct gray level regions of the image. It should be noted that many Gradient and Laplacian operators such as Roberts [4], Canny [5], Prewitt [6], Sobel [7], and others, have been presented for classical edge detection. And these operators based edge detection methods are listed as follows: (a) Cellular Automata [8] (b) particle swarm optimization (PSO) [9] (c) Wavelet [10], (d) Anisotropic Gaussian Kernels (AGK) [11], (e) Ant colony optimization (ACO) [12]. Besides, the swarm intelligence-based ACO algorithm has been offered by Dorigo et al. and it was motivated by the universal collective behavior of ants in the present environment [13], an important method derived from the development of ACO modifications. Zhang et al. suggested topology-preserving 3D image segmentation based On hyperelastic regularization [14]. The authors Liu and Li [15] recommended a fabric defect detection technique based on the aspect of low-rank decomposition with structural constraints. Further information on edge detection method through active contour without edge has also been available in the literature [16]. In addition, new edge detection approaches have been published in peer-reviewed journals [17]. The main limitations of the edge detection algorithms include illumination sensitivity, noise sensitivity, and unadjusted parameters, according to [18, 19]. Hence, there are distinct edge detection methods that have so far been framed to reduce the limitations of the aforementioned edge detection approaches while maximizing their enforcement [20]. Methods

of edge detection based on the fuzzy notion, which have some difficulties in the formation of fuzzy rules. The use of NS-based edge detection helps to alleviate these issues. Just a few works are done in NS based framework and it exposes the originality of the current research. Therefore, the goal of this research is to contribute to future studies that use NS for segmentation and edge detection.

In this continuation, the Neutrosophic Set (NS) was discovered by the premise of Neutrosophy theory and it was first introduced by Florentin Smarandache in the year 2003 [21]. With the help of the NS approach, the origin, scope, and nature of neutralities are discussed. NS is a new philosophical branch [22] and it is a recent method that successfully addresses the problem of vagueness and indeterminacy in circumstances [23] such as biomedical, stock exchange, weather, law, and so on. Hence, the NS domain act as a decision support system in order to overcome the limitations of vagueness. Nonetheless, the neutrosophication functions and their application by MATLAB were recommended by the authors, Bakro et al. [24]. Meanwhile, the same authors offered the neutrosophic method to digital images in their paper [25]. However, NS has been applied successfully in a wide range of domains, including filtering, image processing, segmentation, edge detection, and so on. For remarkable efficiencies in the analysis of neutrosophic information, neutrosophic-based edge detection of medical images is a specialized area of research.

In the literature, only a few works can be obtained from the premise of NS-based segmentation technique [26], which is a popular segmentation methodology for obtaining indeterminate situations of the images, where the indeterminacy of the image is approximated by disturbances like noise, low quality of an image, and so on. This method leads to the problem of uncertainties and inconsistent information. According to [27], the authors used Chan-Vese approaches and NS to segment the images. Dhar and Kundu [28] utilized the two concepts like NS and digital shearlet transform (DST) to segment (text region) the images. Antera and Hassenian (2018) [29] designed an NS segmentation framework for CT liver tumors by using the fast fuzzy C-means algorithm (FFCM) and particle swarm optimization (PSO). We were able to obtain a better CT image with less noise by using NS-based pre-processing. Guo et al. (2017) [30] demonstrated the new method to identify the myocardial contrast of the myocardial echocardiography in the left ventricle and the method is computed by combining two strategies such as active contour method and neutrosophic similarity score. Besides that, employing chest X-ray images, Yasser et al [31]. developed a hybrid automated intelligent COVID-19 classification based on Neutrosophic logic and machine learning approaches. Singh, after that, proffered a multiple thresholding technique depending on type-2 neutrosophic entropy-fusion for the classification of brain tumor tissue structures [32]. Following that, Dhar [33] described

a technique for accurately sectioning multi-class images using weak continuity constraints and a neutrosophic set.

In addition, Mehrdad et al. [34] formed a new framework and it is applied in the liver dome in which the liver is automatically detected by utilizing the random walker method. The authors of [35] devised a multi-atlas extraction method for fast automated (with/without abnormality) liver image segmentation from computational tomography angiography (CTA) and this method contains the local decision fusion. Platero et al. [36] constructed a unique segmentation process, it is to extract the liver image from a CT scan, where the process is formed by the combination of an affine probabilistic atlas, low-level operations, and a multi atlas-based segmentation. Li et al. [37] presented the automatic 3D (liver) object extraction procedure, which is to divide the Object and Background of the image via the concept of convolution neural network and the graph cut. In [38], the author proposed the thyroid nodule segmentation process and it is fundamentally based on the perspective like level-sets and spatial information with clustering. Further, Salah et al. [39] suggested a new method based on the convolutional neural network for human skin detection.

On the other hand, MR image analysis has become a remarkable research field due to the rapid advancement in computer vision and image analysis techniques. However, due to the presence of objects that are inconsistent with their edges and textures, it is necessary to develop a method of recognition and vision for MR images but it is complicated. In order to address this issue, many researchers are now focusing their greater efforts on the separation approach. The varying distribution of gray level pixels can be applied to distinguish various areas (i.e., gray matter, white matter, and cerebrospinal fluid) of the MR image separation. The MR image separation has gone through various incarnations since its advances. In addition, extraction of gray matter into the spine, Datta et al. [40] a threshold-based technique (TBT) is furnished, that is primarily based on the morphological geodetic active contour (MGAC) technique. Taheri et al. [41] advised TBT for extracting the tumor, which has been based on the technique in a level set. The authors [42] recommended an automated and adaptive technique for extracting the MR image of the liver vessels. For the past few decades, MR image analysis is not examined in terms of NS theory.

Inspired by the before talks and compared to the present research accomplishments, the great contributions of this study are suggested by being given at the upcoming points.

- (1) As a first attempt, the NS-based edge detection system is framed in this research article for images with not only noises but also unstable situations. The concept of NS, NS-based entropy, and the fusion rule were combined in the design of NS to create a new fusion mechanism.

- (2) A new powerful edge detection methodology for finding edges in the fused images is elaborated in a supervised manner, and it ensures the rejection of disturbances inclusive of noise and unstable information. The proposed NS-based edge detection method can be easily implemented, and it has the amount of truth, false and indeterminant degrees that is simply obtained through a combination of Bell Shaped (BS) function, Sobel operator, and Neutrosophic Theory.
- (3) The resulting subsets are changed into the form of binary using the threshold values and these values of threshold are calculated by applying different entropies such as Norm, Threshold, Sure, and Shannon. Applying the morphological operations on the generated images, then acquire the edge detected images.
- (4) For the experimental purposes, distinct performance measurement factors such as FOM and PSNR are employed. Ultimately, the statistical values, including comparative research, are provided to reveal the efficacy of the Norm entropy-based image edge detection scheme introduced in this work.
- (5) Additionally, the aforementioned method has been compared to some of the methods found in the literature via Sobel [7], Tian [13], Chan [16], and Wu [18]. As a result, these process activities demonstrated the reliability of the industry and the systematic superiority of the proposed method.

The scheme of the research paper is arranged below. Section 2 gathers the theoretical background of NS, which consists of some subsections such as Basics of neutrosophy, Preprocessing, Neutrosophic image fusion, and Neutrosophic edge detection. Section 3 presents the performance measurement factors. Section 4 describes the statistical findings of the present work in terms of NS-based edge detection of different images. Lastly, numerous closing quotes are briefly showed in the final section.

2. Theoretical Background

2.1. *Basics of Neutrosophy*

Smarandache [21] firstly initiated the new idea of neutrosophy motivated by the aspect of philosophical precedence, which simultaneously separates each concept from a certain degree of truth, falsity, and indeterminacy. Since, neutrosophy has laid solid foundations for new mathematical theories such as NS, neutrosophic probability, neutrosophic logic, and neutrosophic statistics. In this, each statement is evaluated as belonging to the amount of true subset T , false subset F , and indeterminant subset I , respectively. The NS holds some sets like the dialetheist set, paraconsistent set, fuzzy set, tautological set, and intuitionistic fuzzy set. In a multidisciplinary way, NS has solved many problems. Further, neutrosophic logic delivers the

structure of neutrosophic connectives such as conjunction, negation, and disjunction. Furthermore, the neutrosophic images are mathematically formulated and it is being shown in the upcoming part of the research article.

Moreover, MR brain changes can be noticed in terms of gray matter, white matter, and cerebrospinal fluid. The before-mentioned changes are extremely imprecise and cannot be exactly specified at the idea of probability computation. Since NS theory can be recognized as a suitable approach. This explains some of the ambiguities and these ambiguities correlated with the MR images can be represented with three distinct membership degrees. In this, MR brain image is split into three subsets respectively, T , F , and I in the NS domain. The subset T specifies the image object, the subset F describes the image background and the subset I refers to the image edge. Figure. 1 exhibits the flow diagram of the NS-based image edge detection process. In Figure. 1, the test image can be initially transferred to grey scale form, then the gray image is processed (removing disturbances) by employing a median filter. As a result, the filtered image is changed into the NS domain (partitioned into T , F , and I subsets). Later, NS-based entropy is implemented on these subsets to create a new image. Moreover, the gained image is decomposed into the blocks and applies the fusion rule to form a neutrosophic fused image. Then the obtained image is processed by edge detection. In the flow chart 1, the object having the edges is gained at the final stage.

2.2. *Preprocessing*

The initial image (original) changes to a grayscale domain by using direct Matlab code and then it is drained by applying a median filter (MF). MF is a noise removal approach that helps to eliminate the disturbances in the image and gives exclusive results in the image segmentation process. This offers a superior noiseless edge detected image during the segmentation process. Additionally, it protects the features of the edges in the image. More number of filters were available in the literature but this study preferred MF, because of the simplest one and it yields good results in our edge detection mechanism.

2.3. *Neutrosophic image fusion*

To employ NS design for image processing, the image must be converted to a neutrosophic field. Particularly, we expand an NS-based image processing system that selects three degrees via., one for the T and the others F and I . They are degrees of truth, false and indeterminate subsets respectively. In consequence, a test image ($\mathbb{T}\mathbb{I}$) whose length is specified by the symbol ' l ' and the width is symbolized by ' w '. Each image element $\mathbb{T}\mathbb{I}(l, w)$ in the image is reset by a neutrosophic field design [21], and that can be visualized by the following format: $\mathbb{T}\mathbb{I}_{NS} = \{T(l, w), F(l, w), I(l, w)\}$ or $\mathbb{T}\mathbb{I}_{NS} = \mathbb{T}\mathbb{I}(t, f, i)$, where the image element t indicates the true

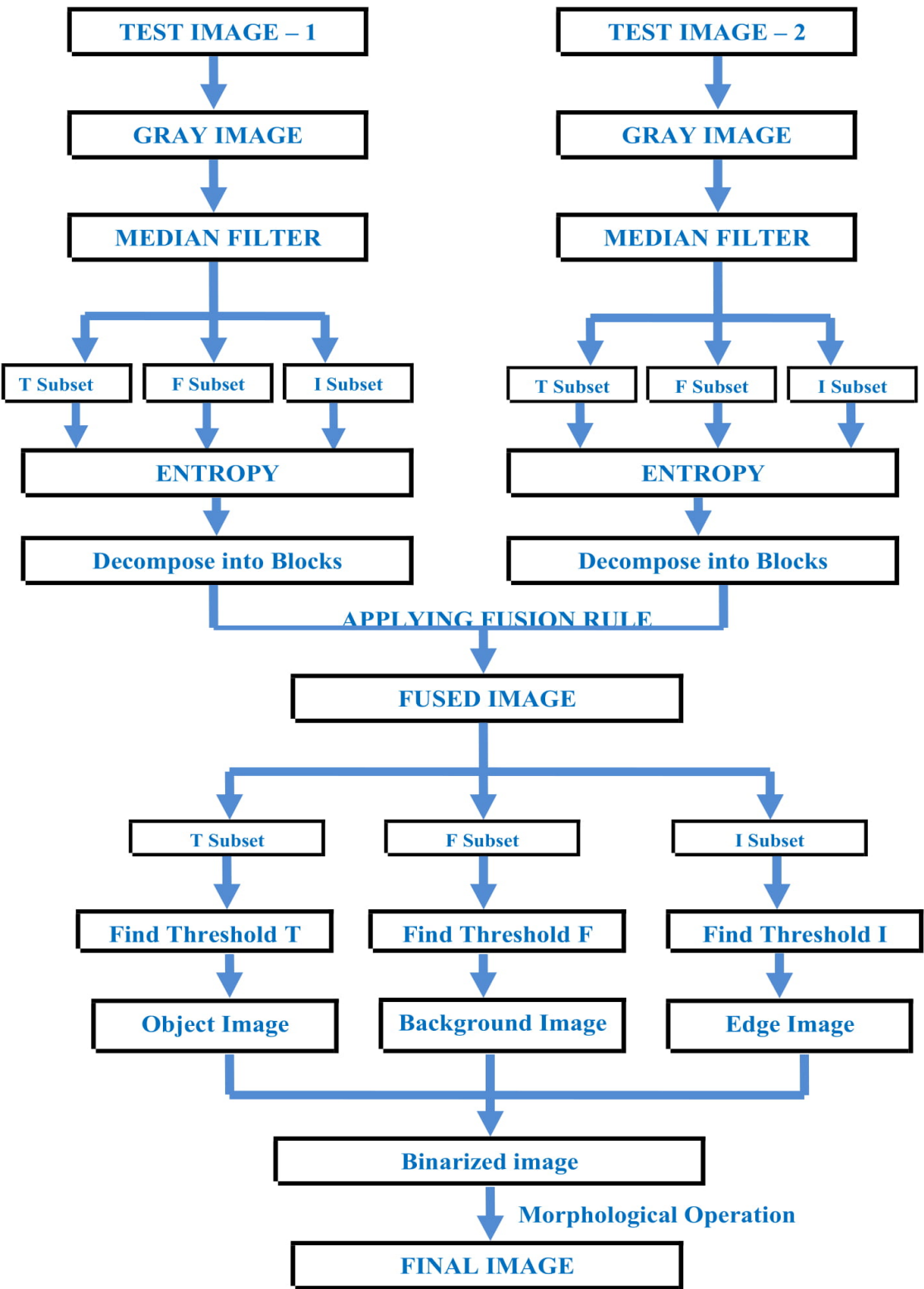


FIGURE 1. Flowchart of the proposed mechanism

subset, f mentions the false subset and i refers the indeterminate subset. Here, t differs in the white pixel set T , f varies in the black pixel set F and i fluctuate in the noise pixel set I . These are described as follows:

$$T(l, w) = \frac{\mathbb{G}(l, w) - \mathbb{G}_{min}}{\mathbb{G}_{max} - \mathbb{G}_{min}} \quad (1)$$

$$F(l, w) = 1 - T(l, w) \quad (2)$$

$$I(l, w) = \sqrt{T(l, w)^2 + F(l, w)^2} \quad (3)$$

In equ (1), the notations \mathbb{G}_{max} , \mathbb{G}_{min} , respectively depicts the maximum and minimum values of the image ($\mathbb{T}\mathbb{I}$) also the symbol $\mathbb{G}(l, w)$ indicates the $(l, w)^{th}$ gray level of the test image. Then, each image element (l, w) belongs to the image ($\mathbb{T}\mathbb{I}$), which can then be defined as NS using the aforementioned equation. For this depiction, the maximum and minimum values from the gray level \mathbb{G} in the image ($\mathbb{T}\mathbb{I}$) are applied, and they can be derived from \mathbb{G}_{min} and \mathbb{G}_{max} . The main benefit of those received formulas is that they can control truth, false, and indeterminate subsets between the ranges 0 and 1. Combining the previously obtained neutrosophic components (T , F , and I) can provide complete information about inherited uncertainty at the problem space. Now, the entropy can be applied to compute an inherited ambiguity in indefinite circumstances. If such ambiguities are reported using NS, their estimation is also achievable from entropy. The neutrosophic entropy information (NEI) function [43] is used for this specific purpose, which can determine the values of each Neutrosophic Information ($\mathbb{N}\mathbb{I}$) entropy and it is illustrated as follows.

The function $\mathbb{ENT}(\mathbb{N}\mathbb{I}) : \mathbb{ENT}(\mathbb{N}\mathbb{I}) \rightarrow [0, 1]$ is known as NEI of an $\mathbb{N}\mathbb{I}$, it can be signified by the following design

$$\mathbb{ENT}(\mathbb{N}\mathbb{I}) = 1 - \frac{1}{3} \sum_{l, w \in \mathbb{G}} (T(l, w) + F(l, w) + I(l, w)) \times E_1 E_2 E_3 \quad (4)$$

Where, $E_1 = |T(l, w) - T^c(l, w)|$, $E_2 = |F(l, w) - F^c(l, w)|$, $E_3 = |I(l, w) - I^c(l, w)|$, $T^c = F(l, w)$, $F^c = T(l, w)$ and $I^c = 1 - I(l, w)$.

2.3.1. NS-based image fusion algorithm

The image fusion algorithm is drawn by the notion of NS [21], which is augmented by the upcoming steps.

- (1) The representation of two test images given by $\mathbb{T}\mathbb{I}_1$ and $\mathbb{T}\mathbb{I}_2$. These test images have \mathbb{L} levels of grayness and $\mathbb{G}(l, w)$ is the intensity of the image element at the particular position (l, w) , where the (l, w) varies from 0 to 255. The test images can be written

in the following matrix design.

$$\mathbb{T}\mathbb{I}_1 = \begin{bmatrix} \mathbb{G}(1,1) & \mathbb{G}(1,2) & \cdots & \mathbb{G}(1,w) \\ \mathbb{G}(2,1) & \mathbb{G}(2,2) & \cdots & \mathbb{G}(2,w) \\ \vdots & \vdots & \ddots & \vdots \\ \mathbb{G}(l,1) & \mathbb{G}(l,2) & \cdots & \mathbb{G}(l,w) \end{bmatrix} \quad (5)$$

Here, ' l ' and ' w ' signifies the length and width of the test image $\mathbb{T}\mathbb{I}_1$ and $\forall \mathbb{G}(l,w) \in \mathbb{T}\mathbb{I}_1$.

This formation is same for test image $\mathbb{T}\mathbb{I}_2$.

- (2) At first, each image element ($\forall \mathbb{G}(l,w)$) of the test images characterized individually in $\mathbb{N}\mathbb{I}$ format (this contains true, false and indeterminate degrees) that can be mathematically encoded as $\mathbb{N}\mathbb{I}(l,w)$, which is defined by the following matrix form.

$$\mathbb{T}\mathbb{I}(\mathbb{N}\mathbb{I}) = \begin{bmatrix} \langle T(1,1), F(1,1), I(1,1) \rangle & \langle T(1,2), F(1,2), I(1,2) \rangle & \cdots & \langle T(1,w), F(1,w), I(1,w) \rangle \\ \langle T(2,1), F(2,1), I(2,1) \rangle & \langle T(2,2), F(2,2), I(2,2) \rangle & \cdots & \langle T(2,w), F(2,w), I(2,w) \rangle \\ \vdots & \vdots & \ddots & \vdots \\ \langle T(l,1), F(l,1), I(l,1) \rangle & \langle T(l,2), F(l,2), I(l,2) \rangle & \cdots & \langle T(l,w), F(l,w), I(l,w) \rangle \end{bmatrix}$$

(OR) (6)

$$\mathbb{T}\mathbb{I}(\mathbb{N}\mathbb{I}) = \begin{bmatrix} \mathbb{N}\mathbb{I}(1,1) & \mathbb{N}\mathbb{I}(1,2) & \cdots & \mathbb{N}\mathbb{I}(1,w) \\ \mathbb{N}\mathbb{I}(2,1) & \mathbb{N}\mathbb{I}(2,2) & \cdots & \mathbb{N}\mathbb{I}(2,w) \\ \vdots & \vdots & \ddots & \vdots \\ \mathbb{N}\mathbb{I}(l,1) & \mathbb{N}\mathbb{I}(l,2) & \cdots & \mathbb{N}\mathbb{I}(l,w) \end{bmatrix}$$

- (3) Thereafter, each $\mathbb{N}\mathbb{I}(l,w)^{th}$ values of test images $\mathbb{T}\mathbb{I}_1$ and $\mathbb{T}\mathbb{I}_2$ are assessed by the fundamental concept of NEI function in equ (4) and it is generally notified by the symbol is $\mathbb{E}\mathbb{N}\mathbb{T}(\mathbb{N}\mathbb{I}(l,w))$, then their matrix representation is given in the upcoming equation

$$\mathbb{E}\mathbb{N}\mathbb{T}(\mathbb{N}\mathbb{I}) = \begin{bmatrix} \mathbb{E}\mathbb{N}\mathbb{T}(\mathbb{N}\mathbb{I}(1,1)) & \mathbb{E}\mathbb{N}\mathbb{T}(\mathbb{N}\mathbb{I}(1,2)) & \cdots & \mathbb{E}\mathbb{N}\mathbb{T}(\mathbb{N}\mathbb{I}(1,w)) \\ \mathbb{E}\mathbb{N}\mathbb{T}(\mathbb{N}\mathbb{I}(2,1)) & \mathbb{E}\mathbb{N}\mathbb{T}(\mathbb{N}\mathbb{I}(2,2)) & \cdots & \mathbb{E}\mathbb{N}\mathbb{T}(\mathbb{N}\mathbb{I}(2,w)) \\ \vdots & \vdots & \ddots & \vdots \\ \mathbb{E}\mathbb{N}\mathbb{T}(\mathbb{N}\mathbb{I}(l,1)) & \mathbb{E}\mathbb{N}\mathbb{T}(\mathbb{N}\mathbb{I}(l,2)) & \cdots & \mathbb{E}\mathbb{N}\mathbb{T}(\mathbb{N}\mathbb{I}(l,w)) \end{bmatrix} \quad (7)$$

- (4) The entropy values in the above matrix $\mathbb{E}\mathbb{N}\mathbb{T}(\mathbb{N}\mathbb{I}(l,w))$ for the test images $\mathbb{T}\mathbb{I}_1$ and $\mathbb{T}\mathbb{I}_2$ are decomposed into $\mathbf{p} \times \mathbf{q}$ blocks. In general, the \mathbf{m}^{th} blocks of decomposed images are specified by the variables $\mathbb{T}\mathbb{I}_{NS1\mathbf{m}}$ and $\mathbb{T}\mathbb{I}_{NS2\mathbf{m}}$ respectively.
- (5) Evaluate the sum of amount of whiteness and blackness of the two associated blocks.
- (6) Each block is combined with each other with the help of the following fusion rule

$$\mathbb{T}\mathbb{I}_{NS\mathbf{m}}(l,w) = \begin{cases} \min\{\mathbb{T}\mathbb{I}_{NS1\mathbf{m}}(l,w), \mathbb{T}\mathbb{I}_{NS2\mathbf{m}}(l,w)\}, & \text{if } \text{count}(\text{blackness}) < \text{count}(\text{whiteness}) \\ \max\{\mathbb{T}\mathbb{I}_{NS1\mathbf{m}}(l,w), \mathbb{T}\mathbb{I}_{NS2\mathbf{m}}(l,w)\}, & \text{if } \text{count}(\text{blackness}) > \text{count}(\text{whiteness}) \\ \frac{\mathbb{T}\mathbb{I}_{NS1\mathbf{m}}(l,w) + \mathbb{T}\mathbb{I}_{NS2\mathbf{m}}(l,w)}{2}, & \text{otherwise} \end{cases} \quad (8)$$

Here, max & min in equ (8) indicate the maximum and minimum actions on the NS domain images respectively.

- (7) The gained blocks are re-modeled to an image, then attain a fused neutrosophic image without ambiguities.
- (8) In the previous step, the neutrosophic image was discovered, and then the image was regenerated to the crisp format (\mathbb{I}_{Fused}), by applying the reverse function of Equ (1).

2.4. Neutrosophic Edge detection

2.4.1. The procedure for finding T and F subsets

By introducing the design of bell-shaped function (BS-function), which acts as a suitable and a virtual soft computer tool for addressing the brightness level of the gray image, hence studies of BS-function are growing rapidly in many realistic areas [27]. Here, the BS-function is employed to fused image (\mathbb{I}_{Fused}), as a result of T subset is found out. According to the design of BS-function, the mathematical formulation of neutrosophic T subset is explored below.

$$T(l, w) = \pi(\mathbb{I}_{Fused}(l, w), b_1, b_2, b_3, b_4) \begin{cases} 0 & \text{if } 0 \leq \mathbb{I}_{Fused}(l, w) \leq b_1 \\ \frac{(\mathbb{I}_{Fused}(l, w) - b_1)^2}{(b_4 - b_1)(b_4 - b_1)} & \text{if } b_1 \leq \mathbb{I}_{Fused}(l, w) \leq b_2 \\ 1 - \frac{(\mathbb{I}_{Fused}(l, w) - b_2)}{(b_4 - b_3)(b_4 - b_3)} & \text{if } b_2 \leq \mathbb{I}_{Fused}(l, w) \leq b_3 \\ \frac{(\mathbb{I}_{Fused}(l, w) - b_4)^2}{(b_4 - b_3)(b_4 - b_3)} & \text{if } b_3 \leq \mathbb{I}_{Fused}(l, w) \leq b_4 \\ 0 & \text{if } \mathbb{I}_{Fused}(l, w) > b_4 \end{cases} \quad (9)$$

$$F(l, w) = 1 - T(l, w) \quad (10)$$

Where $\mathbb{I}_{Fused}(l, w)$ denotes the grayness of $(l, w)^{th}$ pixel of the fused image \mathbb{I}_{Fused} . The input parameters b_1, b_2, b_3 and b_4 of the BS-function computes the shape of the function. The action of the BS-function is shown in Algorithm 1.

Obtaining b_1, b_2, b_3 and b_4 Parameters: The parameters b_1, b_2, b_3 and b_4 are to be computed by employing a histogram based method as explored below:

- (1) Compute the histogram of the (\mathbb{I}_{Fused}) fused image.
- (2) Obtain local maxima of the histogram
 $\mathbb{I}_{Fused}\max(g_1), \mathbb{I}_{Fused}\max(g_2), \mathbb{I}_{Fused}\max(g_3), \dots, \mathbb{I}_{Fused}\max(g_n).$
- (3) Obtain the mean of local maxima
 $\overline{\mathbb{I}_{Fused}\max} = \left(\sum_{i=1}^N \mathbb{I}_{Fused}\max(g_i) \right) / N$
- (4) Evaluate (peak values $\mathbb{I}_{Fused}\max$) then
 $b_2 \leftarrow \text{First peak value}$
 $b_3 \leftarrow \text{Last peak value}$

Algorithm 1 BS-Function Algorithm

```

1: if  $0 \leq \mathbb{I}_{Fused}(l, w) \leq b_1$  then

2:    $T(l, w) \leftarrow 0$ 

3: else if  $b_1 \leq \mathbb{I}_{Fused}(l, w) \leq b_2$  then

4:    $T(l, w) \leftarrow \frac{(\mathbb{I}_{Fused}(l, w) - b_1)^2}{(b_4 - b_1)(b_4 - b_1)}$ 

5: else if  $b_2 \leq \mathbb{I}_{Fused}(l, w) \leq b_3$  then

6:    $T(l, w) \leftarrow 1 - \frac{(\mathbb{I}_{Fused}(l, w) - b_2)}{(b_4 - b_3)(b_4 - b_3)}$ 

7: else if  $b_3 \leq \mathbb{I}_{Fused}(l, w) \leq b_4$  then

8:    $T(l, w) \leftarrow \frac{(\mathbb{I}_{Fused}(l, w) - b_4)^2}{(b_4 - b_3)(b_4 - b_3)}$ 

9: else if  $\mathbb{I}_{Fused}(l, w) > b_4$  then

10:   $T(l, w) \leftarrow 0$ 

11: end if

12: end if

```

(5) Find out the standard deviation (*std*) of the fused image

$$std = \left(\frac{1}{N} \sum_{i=1}^N (\mathbb{I}_{Fused}(i) - \overline{\mathbb{I}}_f)^2 \right)^{1/2}, \text{ where } \overline{\mathbb{I}}_f = \frac{1}{N} \sum_{i=1}^N \mathbb{I}_{Fused}(i)$$

(6) Obtaining the values of b_1 and b_4 are given below

$$b_1 \leftarrow b_2 - std$$

$$b_4 \leftarrow b_3 + std.$$

2.4.2. The procedure for finding *I* subset

The neutrosophic subset *I* was determined by utilizing Zhang et al. [11] method. One of the significant research domains is Homogeneity (*homo*) because it plays a vital role in edge detection schemes, and it is correlated with local information. In some situations like background transitions, color transitions, and edge regions, this domain (*homo*) value is increased. Algorithm 2 refers to the process for determining the *I* subset. The *homo* consists of two main parts such as standard deviation (*std.div*) and the discontinuity (*dis*) of the gray level pixels. The *std.div* is one of the most effective methods for representing the contrast level of the pixels, whereas the changes in the gray pixels are symbolized in *dis*. The *std.div* and *dis* are enumerated at beginning of algorithm 2. The edge values are illustrated by utilizing the

dis of the pixel (l, w) . The Sobel operator is a frequently used system to provide dis of a pixel in the image due to its appropriateness.

Algorithm 2 The process of obtaining the I subset

1: Determine the each coordinate pixel $(l, w)^{th}$ $std.div$ of the \mathbb{I}_{Fused} image is given by

$$std.div(l, w) = \sqrt{\frac{\sum_{p=l-(D-1)/2}^{l+(D-1)/2} \sum_{q=w-(D-1)/2}^{w+(D-1)/2} \left(\mathbb{I}_{Fused}(l, w) - \frac{\sum_{p=l-(D-1)/2}^{l+(D-1)/2} \sum_{q=w-(D-1)/2}^{w+(D-1)/2} \mathbb{I}_{Fused}(l, w)}{D^2} \right)^2}{D^2}} \quad (11)$$

2: Illustrate every pixel coordinate $(l, w)^{th}$ dis of the \mathbb{I}_{Fused} image by applying the Sobel operator, which is given below

$$dis(l, w) = \sqrt{G_x^2 + G_y^2} \quad (12)$$

where, G_y and G_x indicates the vertical and horizontal derivatives.

3: Find out the $homo(l, w)$ of each pixel coordinate (l, w) of the \mathbb{I}_{Fused} and it is represented as

$$homo(l, w) = 1 - \frac{std.div(l, w)}{max(std.div)} \times \frac{dis(l, w)}{max(dis)} \quad (13)$$

4: Compute the indeterminant subset $I(l, w)$ of the \mathbb{I}_{Fused} image and it is defined by

$$I(l, w) = 1 - homo(l, w) \quad (14)$$

2.4.3. Finding binarized T , F and I Subsets

The computed subsets T , F , and I (previous step) are in the grayscale domain, hence the subsets are transformed into a binarized form (Black and White image) by employing the threshold values. The thresholds are an important and main kind of tool in segmentation schemes and they perform automatically and spontaneously in image processing. The threshold values are directly determined by the following entropies.

Implemented entropy types:

In our segmentation process, some specific entropies are considered to estimate the threshold value within the subsets T , F , and I . Then, the edge detection assessment is tested in terms of selected entropies. The implemented entropies are namely Norm, Threshold, Sure, and Shannon. The mathematical design of these entropies is displayed in the upcoming points.

$$(1) \text{ Norm Entropy} = \frac{1}{L \times W} \sum_{l=1}^L \sum_{w=1}^W |T(l, w)|^p, \text{ where } 1 \leq p < 2$$

- (2) Threshold Entropy = $\frac{1}{L \times W} \sum_{l=1}^L \sum_{w=1}^W \begin{cases} Thres(l, w) = 1 & \text{if } |T(l, w)| > \epsilon \\ Thres(l, w) = 0 & \text{if } |T(l, w)| \leq \epsilon \end{cases}$, where ϵ is a positive threshold value.
- (3) Sure Entropy = $\frac{1}{L \times W} \sum_{l=1}^L \sum_{w=1}^W \begin{cases} Sure(l, w) = \min(T^2(l, w), \epsilon^2), & \text{if } |T(l, w)| \leq \epsilon \\ Sure(l, w) = 0, & \text{otherwise} \end{cases}$, where ϵ is a positive threshold value.
- (4) Shannon Entropy = $\frac{-1}{L \times W} \sum_{l=1}^L \sum_{w=1}^W T^2(l, w) \cdot \log_2(T^2(l, w))$

The same points are repeated in the remaining subsets F and I to get all threshold values of the subsets T , F , and I . The variables *Object*, *Edge* and *Background* are received in this step. The process of these variables is depicted in Algorithm 3. In this segmentation analysis, the respective parameters T_t , F_f , and I_i are implemented for *Object*, *Edge* and *Background* variables to be acquired. The threshold values of the parameters T_t , F_f and I_i are determined with the help of neutrosophic subsets (T , F , I) and before mentioned four entropies. Subsequently, the \mathbb{I}_{Fused} image is divided into three sub-images namely *Object*, *Background* and *Edge* by using the calculated thresholds. The achieved sub-images are combined with each other to get a new \mathbb{I}_{Binary} image, which returns the 0 (Black), 1 (White) values from the image.

2.4.4. Edge detection process

Edge detection is accomplished by using the images \mathbb{I}_{Fused} and \mathbb{I}_{Binary} . The scheme of edge detection is expressed in Algorithm 4. Morphological operations were achieved on the image \mathbb{I}_{Binary} then the edge of the image is acquired. Further, the obtained edges are reassigned to the variable \mathbb{I}_{Edge} . Ultimately, to earn a new edge detected image \mathbb{I}_{ED} , the \mathbb{I}_{Edge} is exaggerated in the fused image, and its edges are detected.

3. Performance measurement factors

In this research, performance measurement factors such as Figure of Merit (FOM), Peak Signal to Noise Ration (PSNR) were taken into account, which was applied to find the success of the edge detection method. The FOM [44] is computed using the given form

$$FOM = \frac{1}{\max(N_{ED}, N_{EA})} \sum_{i=1}^{N_{ED}} \frac{1}{1 + dm^2(i)} \quad (15)$$

Here, the symbols N_{ED} and N_{EA} denote the number of detected edge pixels by the edge detection method and actual edge pixels. The notations $m(i)$ and d respectively denote the closest distance to the actual edge and scaling constant. The FOM value is directly proportional to the quality of the discovered edges. Although the FOM result fluctuates between 0 and 1, the efficiency of edge detection is much better if the above value meets 1.

Algorithm 3 Edge detection process

```

1: If  $(T(l, w) \geq T_t \text{ AND } I(l, w) \geq I_i)$ 
2:    $Object(l, w) \leftarrow \text{true}$ 
3: else
4:    $Object(l, w) \leftarrow \text{false}$ 
5: end
6: If  $(T(l, w) < T_t \text{ OR } F(l, w) \geq F_f) \text{ AND } I(l, w) \geq I_i$ 
7:    $Edge(l, w) \leftarrow \text{true}$ 
8: else
9:    $Edge(l, w) \leftarrow \text{false}$ 
10: end
11: If  $(F(l, w) \geq F_f \text{ AND } I(l, w) \geq I_i)$ 
12:    $Background(l, w) \leftarrow \text{true}$ 
13: else
14:    $Background(l, w) \leftarrow \text{false}$ 
15: end
16: If  $(Object(l, w) \text{ OR } Edge(l, w) \text{ OR } \overline{Background(l, w)}) = \text{true}$ 
17:    $\mathbb{I}_{Binary}(l, w) \leftarrow \text{true}$ 
18: else
19:    $\mathbb{I}_{Binary}(l, w) \leftarrow \text{false}$ 
20: end

```

Algorithm 4 Edge detection algorithm

```

1:  $\mathbb{I}_{Dilation} \leftarrow$  Image dilation activation  $\mathbb{I}_{Binary}$ 
2:  $\mathbb{I}_{Fill} \leftarrow$  Fills the internal gaps on the  $(\mathbb{I}_{Dilation})$  image
3:  $\mathbb{I}_{Clear} \leftarrow$  Extract the connected objects on the  $(\mathbb{I}_{Fill})$  image
4:  $\mathbb{I}_{Skeleton} \leftarrow$  Identify the skeleton image  $(\mathbb{I}_{Clear})$ 
5:  $\mathbb{I}_{Edge} \leftarrow$  Determines the complement of the  $(\mathbb{I}_{Skeleton})$  image
6:  $\mathbb{I}_{ED} \leftarrow$  Fused image  $(\mathbb{I}_{Fused})$ 
7:  $[Length\ Width] \leftarrow$  Computes the  $(\mathbb{I}_{Edge})$  image size
8: for  $l=1:Length$ 
9:   for  $w=1:Width$ 
10:    if  $\mathbb{I}_{Edge}(l, w) \leftarrow 0$ 
11:       $\mathbb{I}_{ED}(l, w, 1) \leftarrow 255$ 
12:       $\mathbb{I}_{ED}(l, w, 2) \leftarrow 0$ 
13:       $\mathbb{I}_{ED}(l, w, 3) \leftarrow 0$ 
14:    end
15:  end
16: end

```

On the other hand, PSNR [45], which was recommended by the author Pratt, is a remarkable factor in evaluating the effectiveness of edge detection. Equ. (16) is the formula used to do the PSNR analysis. PSNR is determined using the formula below.

$$PSNR = 10 \cdot \log_{10} \left[\frac{255^2}{\frac{1}{L \times W} \sum_{l=1}^L \sum_{w=1}^W (N_{EA}(l, w) - N_{ED}(l, w))^2} \right] \quad (16)$$

where L, W specifies the dimensions of the image. $N_{EA}(l, w)$ and $N_{ED}(l, w)$ indicates the $(l, w)^{th}$ image element of the actual edges and the detected image edges obtained by using proposed technique. The largest value of PSNR specifies the high similarity between actual and detected image edges. If the PSNR reaches its minimum, then the similarity will be reduced.

4. Experimental results

In this section, different test images of MR brain were considered for our experiment and are aligned in the proper manner as displayed in Figure. 2. The MR brain medical images were gathered from the link address <http://www.med.harvard.edu/AANLIB/home.html>. The medical images of MR brain (Figure. 2 (A) and 2 (B)) are provided for the purpose of fusion by the proposed fusion technique, and then the fused image result is given in the Figure. 3 (A). The another MR brain images (Figure 2 (C) and 2 (D)) are utilized for the proposed fusion technique and their fused result is presented in the Figure. 3 (B). Similarly, the fusion results of remaining MR brain medical images (Figure 2 (E) - (F), Figure 2 (G) - (H) and Figure 2 (I) - (J)) from the proposed NS-technique were shown in Figure. 3 (C) - 3 (E).

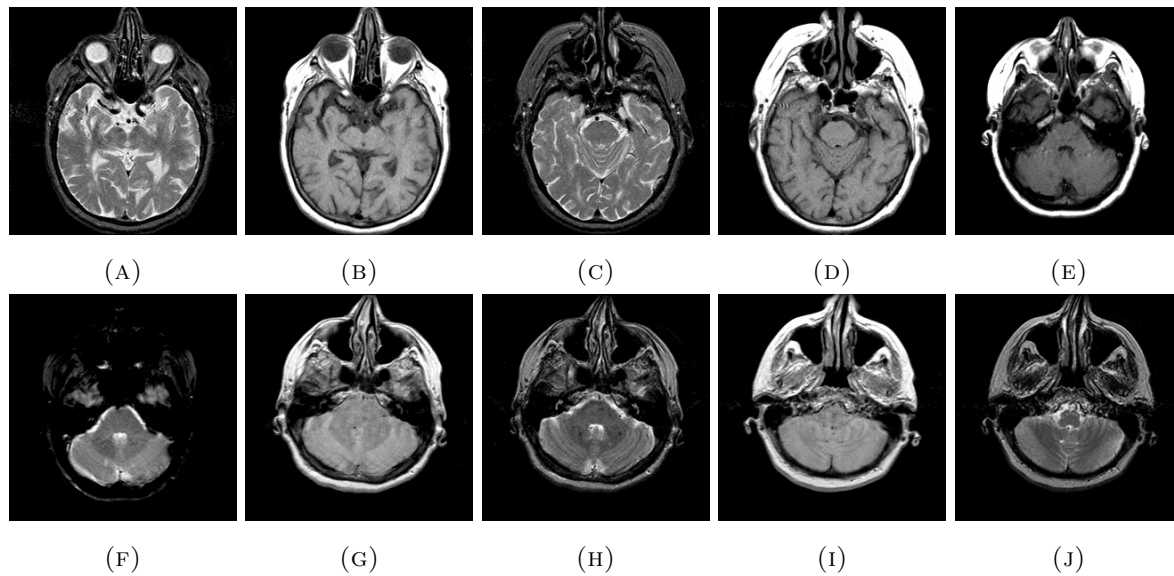


FIGURE 2. Test images of medical MR brain

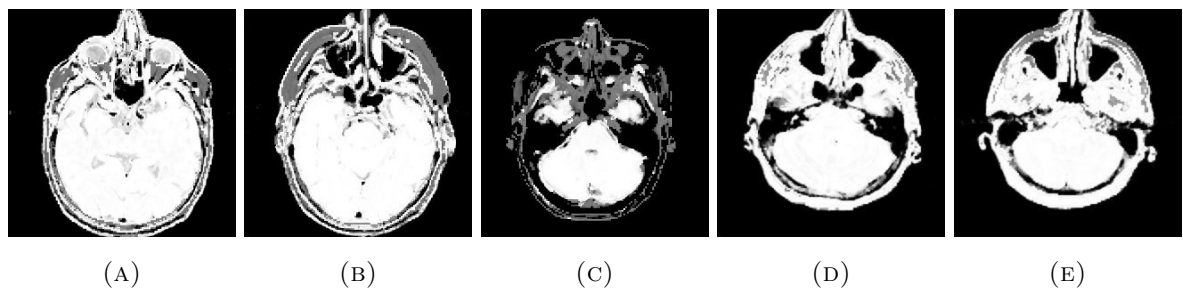


FIGURE 3. Fusion results of medical MR brain images

Norm Results			
Threshold Results			
Sure Results			
Shannon Results			

FIGURE 4. Edge detection of fused image 3(A) using different entropies

4.1. Entropy performance test

To examine the achievement of edge detection for the Norm entropy used in the proposed method, which was compared with some other entropies in NS-based edge detection methods including Threshold, Sure, and Shannon. During this manner, five fused images that are tough to find on the edge are applied. In the initial method analysis, the first fused image of MR

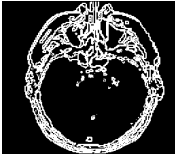
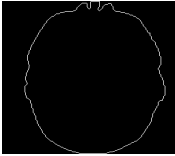
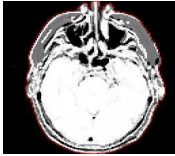


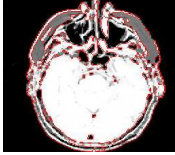
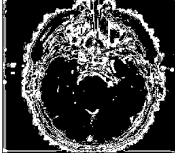
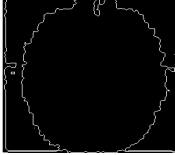
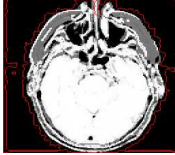
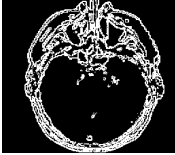

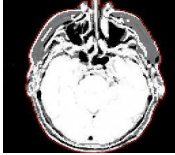
Norm Results			
Threshold Results			
Sure Results			
Shannon Results			

FIGURE 5. Edge detection of fused image 3(B) using different entropies

TABLE 1. The edge detection results for fused images by using FOM and PSNR analysis.

Fused Images	Norm entropy		Threshold entropy		Sure entropy		Shannon entropy	
	FOM	PSNR	FOM	PSNR	FOM	PSNR	FOM	PSNR
Image-1	0.93	33.01	0.86	29.79	0.83	28.94	0.90	31.16
Image-2	0.96	34.20	0.92	32.30	0.90	31.48	0.95	33.40
Image-3	0.91	31.65	0.85	29.48	0.83	28.70	0.83	30.36
Image-4	0.95	33.88	0.91	31.06	0.88	30.52	0.93	32.50
Image-5	0.88	30.85	0.82	28.95	0.80	27.61	0.85	29.99

brain (Figure. 3 (A)) is utilized, which is then converted by a neutrosophic field in terms of three subsets by applying the BS-function and Sobel operator. Then, the subset thresholds of fused MR brain image are calculated by implementing the above four entropies. Further, the subsets are to be generated in the binary form with the help of obtained thresholds for each

TABLE 2. Statistical effects about edge detection results.

	Norm entropy		Threshold entropy		Sure entropy		Shannon entropy	
	FOM	PSNR	FOM	PSNR	FOM	PSNR	FOM	PSNR
Minimum	0.88	30.85	0.82	28.95	0.80	27.61	0.85	29.99
Average	0.93	32.72	0.87	30.32	0.85	29.45	0.89	31.48
Maximum	0.96	34.20	0.92	32.30	0.90	31.48	0.95	33.40

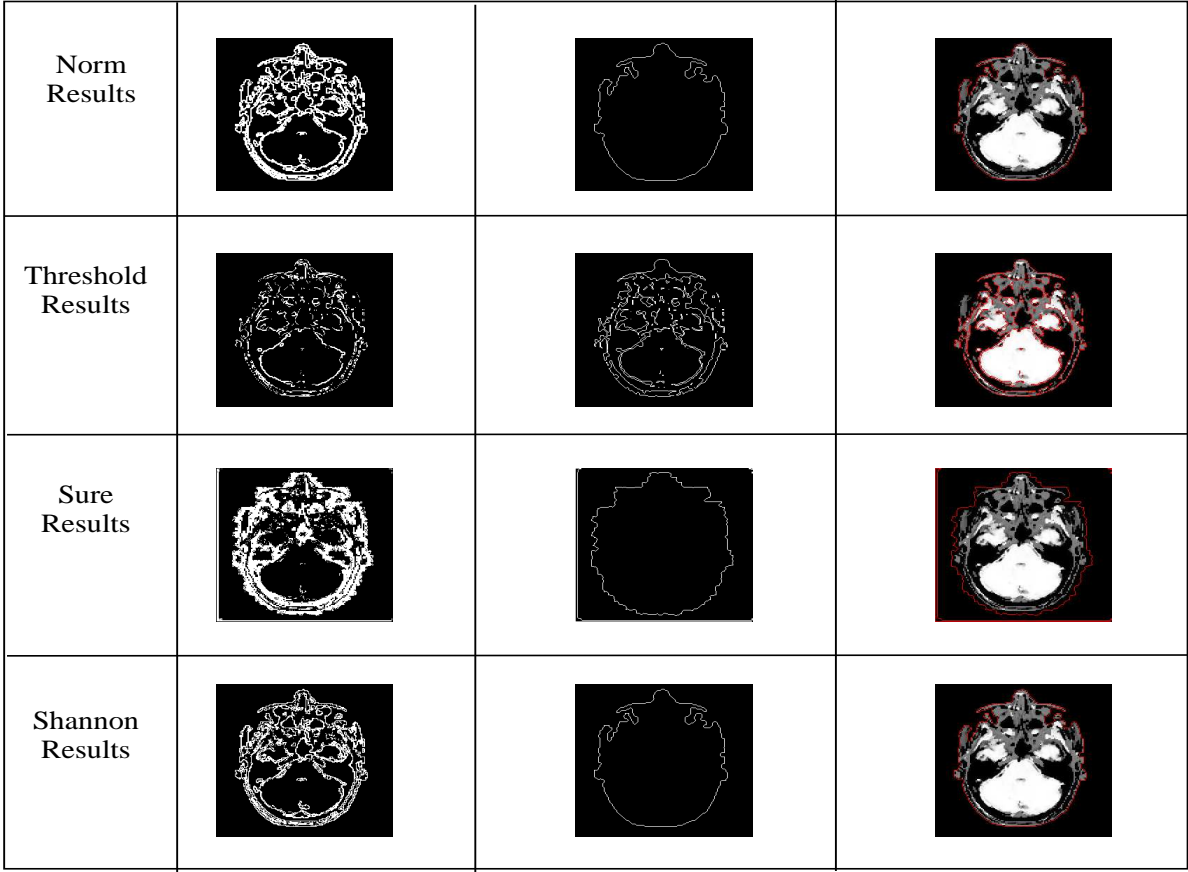


FIGURE 6. Edge detection of fused image 3(C) using different entropies

entropy. By using algorithm 3, the binarised subsets of each entropies were combined with each other in order to obtain \mathbb{I}_{Binary} images, which are presented in the first column of Figure. 4. Furthermore, the morphological operations are executed in the obtained \mathbb{I}_{Binary} images, and the detected results are also shown in the last column of the Figure. 4. In addition, the performance measurement factors such as FOM, and PSNR were analyzed for the edge detected images at different entropies to confirm edge detection performance. The statistical values of the performance measurement factors with different entropies of the proposed mechanism are

TABLE 3. The edge detection results for fused images by using FOM and PSNR analysis.

Fused Images	Sobel Method		Tian Method		Chan Method		Wu Method		Proposed Method	
	FOM	PSNR	FOM	PSNR	FOM	PSNR	FOM	PSNR	FOM	PSNR
Image-1	0.89	31.41	0.90	32.29	0.92	32.45	0.93	33.50	0.95	33.88
Image-2	0.90	31.47	0.91	31.94	0.92	32.01	0.94	32.95	0.96	33.58
Image-3	0.89	30.89	0.91	31.87	0.94	33.12	0.95	33.80	0.96	34.20
Image-4	0.81	25.35	0.83	28.70	0.85	28.24	0.86	31.71	0.89	32.66
Image-5	0.86	30.11	0.87	30.43	0.88	30.88	0.91	31.36	0.93	32.92

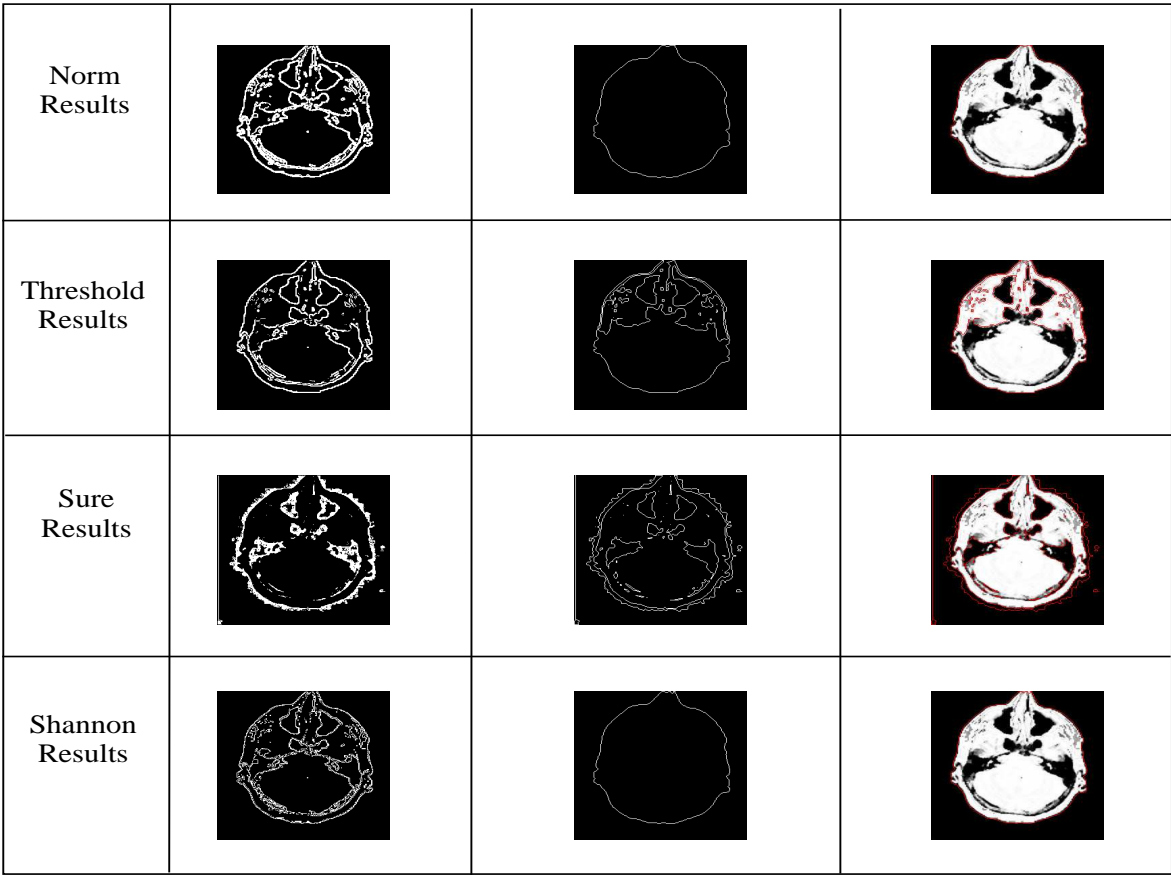


FIGURE 7. Edge detection of fused image 3(D) using different entropies

displayed in Tables 1 - 2. From the Tables. 1 and 2 , the high-performance entropy of the proposed edge detection mechanism is highlighted in bold characters and the tabulated values are plotted in Figures. 10 (a)- 10 (b). At last, Table. 1 and Figure. 10 shows that the

proposed Norm entropy in the edge detection mechanism gives the significant performance with reference to other entropies.

TABLE 4. Statistical effects about edge detection results.

	Sobel Method		Tian Method		Chan Method		Wu Method		Proposed Method	
	FOM	PSNR	FOM	PSNR	FOM	PSNR	FOM	PSNR	FOM	PSNR
Minimum	0.81	25.35	0.83	28.70	0.85	29.24	0.86	31.36	0.89	32.66
Average	0.87	29.85	0.88	31.05	0.90	31.34	0.92	32.67	0.94	33.45
Maximum	0.90	31.47	0.91	31.94	0.94	33.12	0.95	33.80	0.96	34.20



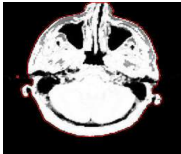
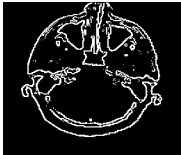

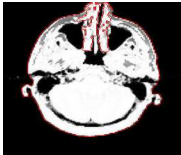



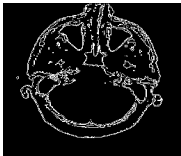

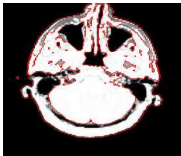
Norm Results			
Threshold Results			
Sure Results			
Shannon Results			

FIGURE 8. Edge detection of fused image 3(E) using different entropies

Subsequently, the second fused image of the MR brain (Figure. 3 (B)) is considered for the edge detection process. Firstly, the taken image is transferred to the domain of NS and it includes the terms of three subsets. Subsets can be calculated using the BS function and the Sobel operator. Each subset threshold value is determined by the concept of the different

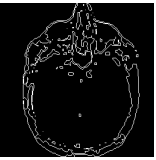
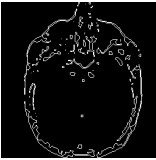
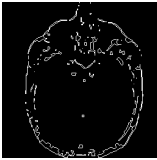
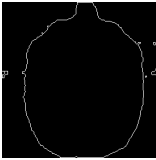

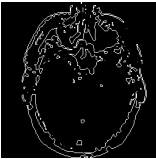
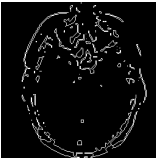
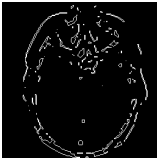
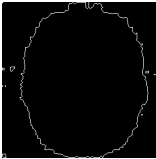



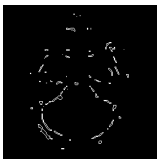
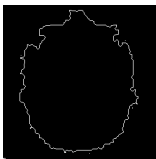




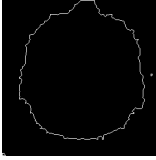



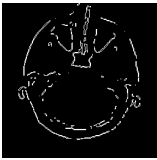
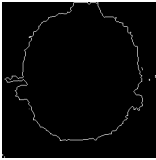

Sobel Method [7]	Tian Method [13]	Chan Method [16]	Wu Method [18]	Proposed Method
				
				
				
				
				

FIGURE 9. Edge detection results for different methods

entropies. Using each entropy threshold value, three subsets are generated by the form of binary images and the resulting images are combined by using algorithm 3 and it produces the new image called as \mathbb{I}_{Binary} . Each entropy of the \mathbb{I}_{Binary} images is exhibited in the first column of the Figure. 5. Moreover, the computed \mathbb{I}_{Binary} images are processed by the morphological operations, and the gained images are shown in the last column of the Figure. 5. Images detected in distinct entropy are intended to confirm the effectiveness of the proposed edge detection by the measurement factors and the statistical values of the measurement factors that are presented in Tables. 1 - 2. The table values (Table 1) of FOM and PSNR are plotted, which are given in Figure. 10 (a) - (b). Finally, the Figures 10 (a) and 10 (b) provide

the result as a Norm entropy with the proposed approach offers higher accuracy than other existing entropy because it offers higher FOM and PSNR values.

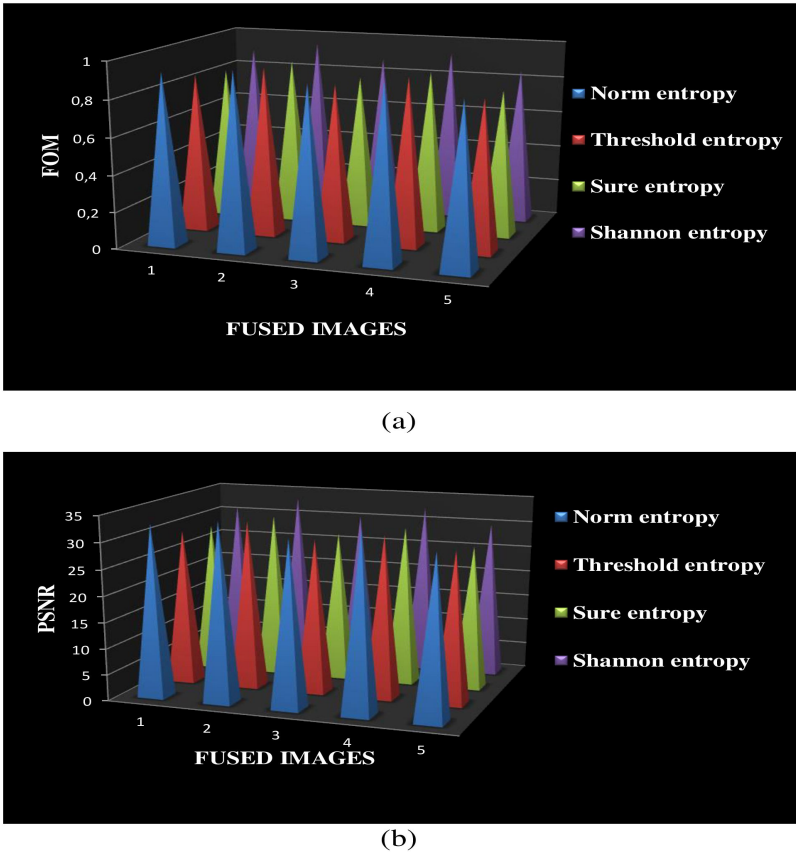


FIGURE 10. Geometric representation of FOM and PSNR analysis for various entropies.

In this continuation, 4 distinct entropies and remaining medical MR brain images are considered for the analysis. The complete information of the previously mentioned test process is employed in the considered images, which are presented in Figure. 2 (E) - 2 (J). At this end, 5 edge detected images were found utilizing the proposed mechanism and these images are given in Figures. 6 - 8. In consequence, the statistical values of the measurement factors in the edge detected images are gained under the proposed edge detection mechanism with 5 MR brain fused images and 4 individual entropies, which are displayed in the aforementioned Tables 1 and 2. In Tables 1 - 2, the Norm entropy produces maximum values in the measurement factors FOM and PSNR values whereas Sure entropy has the minimal FOM and PSNR values.

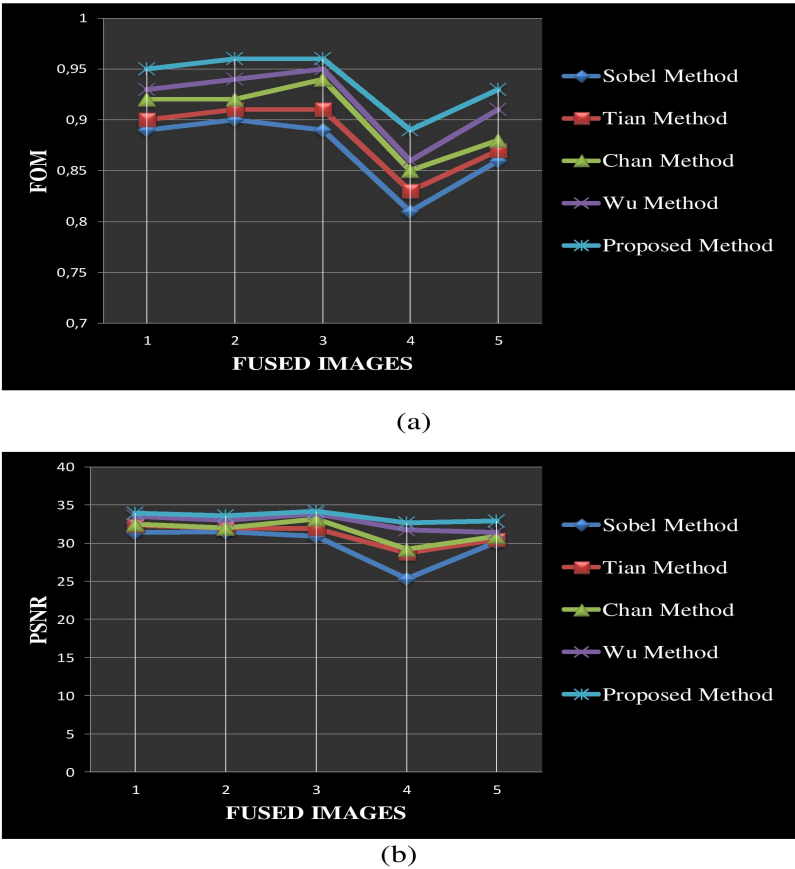


FIGURE 11. Geometric representation of FOM and PSNR analysis for different methods.

Then, the tabulated results (Table 1) of the remaining resultant images are also made available in the Figures. 10 (a) - (b). Thus with the acquired results, it is evidenced that the norm entropy provides constructive performance. While Sure entropy reveals contrast results which have been evidenced in Figure. 10 and Tables. 1 - 2. Hence our study implicates the efficacy of norm entropy as a sustainable tool in the edge detection process of MR brain images.

4.2. Comparative applications of the proposed and different object edge detection methods

Norm entropy with the proposed method was compared to other existing methods which includes Sobel [7], Tian [13], Chan [16] and Wu [18] to assess the proposed edge detection performance. In the aforementioned methods, the edges are seen to be thicker. As a result,

the final image was subjected to morphological operations. To examine the edge detection efficiency, five fused images utilized in entropy analysis were applied, while the five edge detection methods mentioned earlier were employed to these same images. Further, the fused image edges are depicted in Figure 9. The proposed Norm entropy, as shown in Figure. 9, was discovered to be the most effective edge detection method. The performance measurement factors such as FOM and PSNR were executed to compare the real performance of detected edges of the mentioned fused images. Table 3 also includes FOM and PSNR factor data, which are plotted in Figures. 11 (a) - (b), respectively. The proposed method's FOM and PSNR factor values are superior to those acquired by the other four edge detection methods. Moreover, statistical analysis of the FOM and PSNR outcomes earned by the five edge detection methods was performed, and these outcomes are given in Table 4. Also, in Table 4 it can be observed that the minimum, arithmetic average, and maximum values related to the FOM and PSNR effects achieved in the suggested method are larger than the other method. Those effects intimate that this proposed method offers edge detection through a greater level compared via distinct methods.

For the presented Table 2, the average values of the Norm entropy of FOM and PSNR are 0.93 and 32.72, respectively. For these values are larger compared to the different other entropies that can be recommended that the Norm entropy under NS improves the edge detection efficacy. Similarly, in Table 4 given, the average values based on the proposed method of FOM and PSNR are 0.94 and 33.45 respectively. These results are extremely high when compared to the other methods. The most important finding from the experiment is that the suggested method significantly outperforms other methods in detecting the object's edges because these effects are significantly larger when compared to other methods.

5. Conclusion

In this report, a new edge detection mechanism based on the category of the NS scheme has been nominated. This was achieved by the frame of image fusion with edge detection. This mechanism is capable to handle the uncertainties and indeterminant situations of the images. First, the proposed image fusion has been found with the help of NS structure and fusion rules. As a result, images are reproduced by the NS framework using the BS function and the Sobel operator. The resultant images contain three subsets and their values of the threshold are found using distinct entropies. Afterward, the computed thresholds and the subsets are integrated and it produces a new binarised image. Morphological operations are accomplished in the binarised image then the edges of the image are acquired. The same process acts on each entropy and it presents several detected edges. The efficacy of this mechanism is well established through the measurement factors. The given edge detection scheme is also appropriately implemented when a norm entropy appears. Further, the proposed method based on norm entropy was compared with other methods including Sobel, Chan, Tian, and Wu. According to the statistical results of performance measurement factors such as FOM

and PSNR, the mentioned factor values of the proposed method are greater compared to the other existing four methods, which illustrate the superiority of the proposed mechanism.

In future research, the neutrosophic set and its extensions will be further applied in medical image processing such as image denoising, segmentation, etc.

Acknowledgments

This study was financially supported via a funding grant by Department of Science and Technology (DST)-Promotion of University Research and Scientific Excellence (PURSE) Phase-II, Government of India, New Delhi (Memo No. BU/DST PURSE (II)/APPOINTMENT/515).

Conflicts of Interest

The authors declare no conflict of interest.

References

1. Bhat, S. , Koundal. D. (2021). Multi-focus Image Fusion using Neutrosophic based Wavelet Transform. *Applied Soft Computing*, 106, 107307.
2. Balasubramaniam, P. , and Ananthi, V. P. (2014). Image fusion using intuitionistic fuzzy sets, *Information Fusion*, 20, 21–30.
3. Kakarla, R. , Ogunbona, P. O. (2001). Signal analysis using a multiresolution form of the singular value decomposition. *IEEE Transactions Image Process*, 10(5), 724–735.
4. Rosenfeld, A. (1981). The max Roberts operator is a Hueckel–Type edge detector. *IEEE Transactions on Pattern Analysis and Machine Intelligence*, 3(1), 101-103.
5. Canny, J. A. (1986). A computational approach to edge detection. *IEEE Transactions on Pattern Analysis and Machine Intelligence*, 8(6), 679-698.
6. Seif, A. , Salut, M. M. , and Marsono, M. N. (2010). A hardware architecture of Prewitt edge detection. In *Proceedings of the IEEE conference on sustainable utilization and development in engineering and technology*. IEEE. 99-101.
7. Sobel, J. (1990). *Machine vision for three-dimensional scenes*. New York: Academic Pres.
8. Amrogowicz, S. , Zhao, Y. , and Zhao, Y. (2016). An edge detection method using outer Totalistic Cellular Automata. *Neurocomputing*, 214 , 643-653 .
9. Mahdi, S. , Mengjie, Z. , and Mark, J. (2013). A novel particle swarm optimisation approach to detecting continuous, thin and smooth edges in noisy images. *Information Sciences*, 246(10), 28-51.
10. Tua, G. J. , and Karstoft, H. (2015). Logarithmic dyadic wavelet transform with its applications in edge detection and reconstruction. *Applied Soft Computing*, 26, 193-201.
11. Ming, Z. , Zhang, L. , and Cheng. H.D. (2010). A neutrosophic approach to image segmentation based on watershed method. *Signal Processing*, 90, 1510-1517.
12. Liu, X. , and Fang, S. (2015). A convenient and robust edge detection method based on ant colony optimization. *Optics Communications*, 353, 147-157 .
13. Tian, J. , Yu, W. , Chen, L. , and Ma, L. (2011). Image edge detection using variation-adaptive ant colony optimization. In *Transactions on computational collective intelligence*, Springer. V, 27-40 .
14. Zhang, D. , Lui, L. M. (2021). Topology-Preserving 3D Image Segmentation Based on Hyperelastic Regularization. *J Sci Comput*, 87, 74. <https://doi.org/10.1007/s10915-021-01433-y>.

15. Liu, G. , Li, F. (2021). Fabric defect detection based on low-rank decomposition with structural constraints. *Vis Comput.* <https://doi.org/10.1007/s00371-020-02040-y>.
16. Chan, T. F. , and Vese, L. A. (2001). Active contours without edges. *IEEE Transactions on Image Processing*, 10, 266-277.
17. Martinez, A. Gelb, A. , and Gutierrez, A. (2014). Edge Detection from Non-Uniform Fourier Data Using the Convolutional Gridding Algorithm. *J Sci Comput*, 61, 490-512.
18. Wu, Z. , Lu, X. , and Deng, Y. (2015). Image edge detection based on local dimension: a complex networks approach. *Physica A*, 440 , 9-18 .
19. Thirumavalavan, S. , and Jayaraman, S. (2016). An improved teaching-learning based robust edge detection algorithm for noisy images. *Journal of Advanced Research*, 7(6), 979-989.
20. Er-sen, L. , Shu-long, Z. , Bao-shan, Z. , Yong, Z. , Chao-gui, X. , and Li-hua, S. (2009). An adaptive edge detection method based on the canny operator. In *Proceedings of the IEEE international conference environmental science and information application technology*. IEEE. 265-269.
21. Smarandache, F. (2003). A unifying field in logics neutrosophic logic. neutrosophy, neutrosophic set, neutrosophic probability . USA: American Research Press.
22. Sert, E. (2018). A new modified neutrosophic set segmentation approach. *Comput.Electr. Eng*, 65, 576-592.
23. Abdel-Basset, M. , Manogaran, G. , Mohamed, M. , and Chilamkurt, N. (2018). Three-way decisions based on neutrosophic sets and AHP-QFD framework for supplier selection problem. *Future Generation Computer Systems*, 89 , 19-30.
24. Bakro, M. , Al-Kamha, R. , and Kanafani, Q. (2021). Neutrosophication functions and their implementation by MATLAB program. *Neutrosophic Sets and Systems*, 40(1), 169-178.
25. Bakro, M. , Al-Kamha, R. , and Kanafani, Q. (2020). A Neutrosophic Approach to Digital Images. *Neutrosophic Sets and Systems*, 36, 12-23.
26. Eser, S. , and AVCI, D. (2019). A new edge detection approach via neutrosophy based on maximum norm entropy. *Expert Systems With Applications*, 115, 499-511.
27. Sangeeta, K. S. , and Mrityunjaya, V. L. (2017). Combined endeavor of Neutrosophic Set and Chan-Vese model to extract accurate liver image from CT scan. *Computer Methods and Programs in Biomedicine*, 151, 101-109.
28. Dhar, S. , and Kundu, M. K. (2017). Accurate segmentation of complex document image using digital shearlet transform with neutrosophic set as uncertainty handling tool. *Applied Soft Computing*, 61, 412-426.
29. Antera, A. M. , and Hassenian, A. E. (2018). Computational intelligence optimization approach based on particle swarm optimizer and neutrosophic set for abdominal CT liver tumor segmentation. *Journal of Computational Science*, 25, 376-387.
30. Guo, Y. , Du, G.-Q. , Xue, J.-Y. , Xia, R. , and Wang, Y.-H. (2017). A novel myocardium segmentation approach based on neutrosophic active contour model. *Computer Methods and Programs in Biomedicine*, 142, 109-116.
31. Yasser I. , Abd El-Khalek A. A. , Twakol A. , Abo-Elsoud ME. , Salama A. A. , Khalifa F. (2022). A Hybrid Automated Intelligent COVID-19 Classification System Based on Neutrosophic Logic and Machine Learning Techniques Using Chest X-Ray Images. In: Hassanien AE., Elghamrawy S.M., Zelinka I. (eds) *Advances in Data Science and Intelligent Data Communication Technologies for COVID-19*. *Studies in Systems, Decision and Control*, 378. https://doi.org/10.1007/978-3-030-77302-1_7.
32. Singh, P. (2021). A type-2 neutrosophic-entropy-fusion based multiple thresholding method for the brain tumor tissue structures segmentation. *Applied Soft Computing*, 103, 107119.
33. Dhar, S. , Kundu, M. (2021). Accurate multi-class image segmentation using weak continuity constraints and neutrosophic set. *Applied Soft Computing*, 112, 107759.

34. Mehrdad, M. et al. (2016). Automatic liver segmentation on computed tomography using random walkers for treatment planning. *EXCLI J*, 15, 500.
35. Ding, X , et al. (2016). Fast automated liver delineation from computational tomography angiography, *Procedia Comput. Sci.* 90, 87-92.
36. Platero, C. , Tobar, M. C. (2014). A multiatlas segmentation using graph cuts with applications to liver segmentation in CT scans. *Comput. Math. Methods Med*, 16 Article ID 182909.
37. Lu, F. et al. (2017). Automatic 3D liver location and segmentation via convolution neural network and graph cut. *Int. J. Comput. Assisted Radiol. Surg*, 12(2), 171-182.
38. Koundal, D. , Gupta, S. , and Singh, S. (2016). Automated delineation of thyroid nodules in ultrasound images using spatial neutrosophic clustering and level set. *Applied Soft Computing*, 40, 86-97.
39. Salah, K.B. , Othmani, M. , and Kherallah, M. (2021). A novel approach for human skin detection using convolutional neural network. *Vis Comput.* <https://doi.org/10.1007/s00371-021-02108-3>.
40. Datta, E. , Papinutto, N. , Schlaeger, R. , Zhu, A. , Carballido-Gamio, J. , Henry, R. G. (2017). Gray matter segmentation of the spinal cord with active contours in MR images. *Neuroimage*, 147, 788-799.
41. Taheri, S. , Ong, S. H. , Chong, V. (2010). Level-set segmentation of brain tumors using a threshold-based speed function. *Image Vis. Comput*, 28(1), 26-37.
42. Goceri, E. , Shah, Z. K. , Gurcan, M. N. (2017). Vessel segmentation from abdominal magnetic resonance images: adaptive and reconstructive approach. *Int. J. Numer. Method Biomed. Eng*, 33(4), e2811.
43. Pritpal and Singh. (2020). A neutrosophic-entropy based clustering algorithm (NEBCA) with HSV color system: A special application in segmentation of Parkinson's disease (PD) MR images. *Computer Methods and Programs in Biomedicine*, 189, 105317. <https://doi.org/10.1016/j.cmpb.2020.105317>.
44. Abdou, I. E. , and Pratt, W. K. (1979). Quantitative design and evaluation of enhancement/thresholding edge detectors. *Proc. IEEE*, 67(5), 753-763.
45. Pratt, W. K. (1978). *Digital image processing* . USA: John Wiley and Sons.

Received: Feb 8, 2022. Accepted: Jun 2, 2022